Monte Carlo study of the successive phase transitions in K_2SeO_4 and K_2SO_4 crystals

V. I. Zinenko and N. G. Zamkova

L.V. Kirensky Institute of Physics, 660036 Krasnoyarsk, Russia

(Received 4 January 1996; revised manuscript received 3 June 1997)

Monte Carlo calculations at different temperatures have been performed to study the sequence of order-disorder phase transitions: hexagonal ($P6_3/mmc$) $\Rightarrow$ orthorhombic ($Pnam$) $\Rightarrow$ incommensurate $\Rightarrow$ orthorhombic ($Pna2_1$) in K_2SeO_4 and hexagonal ($P6_3/mmc$) $\Rightarrow$ orthorhombic ($Pnam$) $\Rightarrow$ monoclinic($P2/n$) in K_2SO_4. In the model, the BX_4 group has four equilibrium orientations in a disordered hexagonal phase. The interaction constants between the ordering BX_4 groups are calculated within the framework of the electrostatic model and are a sum of direct octupole-octupole and indirect octupole-dipole forces. The polarizabilities of two structural nonequivalent potassium ions are fitted to the structure of the low-temperature phase. The interaction constants are calculated within 19 coordination spheres and it is shown that there is competition between them. Monte Carlo simulations are carried out on the $N \times N \times N1$ hexagonal three-dimensional lattice ($N=16$, $N1=24$ and $N=24$, $N1=48$). Two types of boundary conditions are used: the periodic one and one with phantom ''spins.'' The simulations yield the experimentally observed sequence of phase transitions in K_2SeO_4. There is good agreement with the experimentally observed transition temperatures and behavior of the thermodynamical properties . In the case of K_2SO_4, the model confirms the observed phase transition from the hexagonal phase to the orthorhombic one, and predicts one more transition to the low-temperature monoclinic phase. [S0163-1829(97)05446-5]

I. INTRODUCTION

Potassium selenate and potassium sulphate belong to a large class of compounds with the general chemical formula $ACBX_4$, where A and C are alkali metals and BX_4 are the tetrahedral group SO_4, SeO_4, CrO_4, $ZnCl_4$, etc. Many compounds of this family undergo a phase transition or a cascade of several phase transitions at lower temperature. Some compounds in a certain temperature range transform into incommensurate modulated phases. There are numerous experimental investigations of these compounds and information concerning the crystal structures, phase diagrams, and behavior of the physical properties near the phase transitions can be found in review papers.[1-3]

It is important to emphasize here that all known crystal structures of these compounds have a common feature; namely, they can be considered as slight distortions of the prototype α-K_2SO_4 structure of D_{6h}^4 ($P6_3/mmc$) symmetry. The difference between the structures of different crystals is caused by the orientations of tetrahedra relative to each other as well as to the crystallographic axes. For realization of the hexagonal phase D_{6h}^4 in these crystals several equilibrium positions of the tetrahedral BX_4 groups are needed. The observed variety of structural phase transitions in this family is associated with the different ordering of the BX_4 groups accompanied by slight ionic displacements. It should be noted that the distortions of all known low-symmetrical phases in the crystals of the family under consideration are determined mainly by the BX_4 orientations.[1-3]

Of all crystals of the $ACBX_4$ family potassium sulphate and potassium selenate are its rare representatives in which the hexagonal phase is observed experimentally at high temperatures.[4,5] With a temperature decrease there are some remarkable differences in the behavior of these crystals.

K_2SeO_4 undergoes four successive phase transitions.[6] Above 745 K it takes α-K_2SO_4 structure and has two formula units in the hexagonal unit cell. Below 745 K it transforms to the β-K_2SO_4 structure and has four formula units in the orthorhombic unit cell (space group $Pnam$). At 130 K it transforms to an incommensurate structure with the modulation vector $\mathbf{q}=(1-\delta)^*\mathbf{c}_0^*/3$, where $\mathbf{c}_0^*$ is the first reciprocal-lattice vector along the pseudohexagonal direction. As the crystal is cooled further, δ decreases and vanishes at 93 K when the system locks into a ferroelectric commensurate phase (F phase, space group $Pna2_1$) whose pseudohexagonal axis is triple that of the room-temperature phase. When cooled further, K_2SeO_4 undergoes another transition at 56 K to a monoclinic phase, the space group of which is still not clear. These phase transitions have attracted extensive experimental efforts (see the review in Refs. 1–3 and references there).

K_2SO_4 has a hexagonal phase above 860 K. Below this temperature it transforms into the same orthorhombic phase $Pnam$. The results of the study of K_2SO_4 behavior with a temperature decrease are contradictive. A phase transition at 56 K was observed by Gesi *et al.*[7] and was suggested to be neither incommensurate nor ferroelectric. In Ref. 8 it was suggested that K_2SO_4 underwent the phase transitions at 140 K into a ferroelectric phase. On the other hand, the structure of this compound was investigated at low temperatures in Ref. 9 and it was shown that K_2SO_4 had the paraelectric phase with space group $Pnam$ up to 15 K.

There are few theoretical studies in which the phase transitions in K_2SeO_4 were considered from the phenomenological as well as microscopical points of view. A simulation study of the static structure for both the P and F phases, the dynamical states of K_2SeO_4 at various temperatures in the $Pnam$ phase, and the transition from the P phase to the F
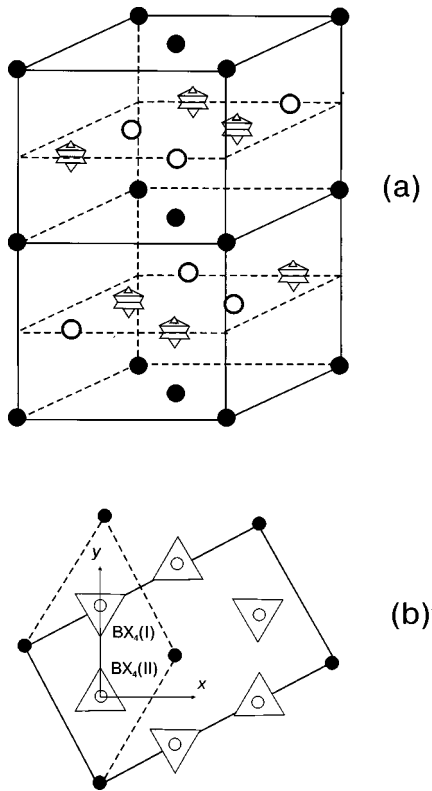
FIG. 1. The crystal structure of the high-temperature phase of $ACBX_4$ (a) and its projection viewed down [001] (b). The triangles represent the BX_4 molecular ions. The A and C metals are shown by open and solid circles.

FIG. 2. Four positions of the BX_4 tetrahedra in the hexagonal phase. Their projection viewed down the [001] plane which crossed the tetrahedra center. The solid and dashed lines indicate the tetrahedra apex above (1,2) and below (3,4) the plane, respectively. The same orientation is denoted both by a number and arrow since for the sake of convenience we used the numbers in the text but the arrows in Table III and the caption to Fig. 8.

phase and to a monoclinic phase at lower temperature using the intra- and intermolecular interactions taken from *ab initio* quantum-chemistry calculations was made quite successfully by Lu and Hardy.[10] The other molecular-dynamics study of K_2SeO_4 (Ref. 11) using the interatomic potential with fitting parameters has been rather successful in reproducing the main features of the hexagonal-orthorhombic and para-ferroelectric phase transitions. These previous studies have stressed the lattice dynamics of this compound and the fact that the dynamical matrix of the system in the *Pnam* phase has the negative eigenvalues. However, in Refs. 10 and 11 a structure of the *I* phase, the phase transition $P \Rightarrow I \Rightarrow F$ and behavior of the thermodynamical properties of K_2SeO_4 near the phase transitions are not discussed.

In the present work for investigation of the phase transitions in K_2SeO_4 and K_2SO_4 the order-disorder model is used. In this model a BX_4 tetrahedron has four equilibrium positions in the hexagonal phase (Fig. 1).

The effective constants of the interaction between the ordered BX_4 tetrahedra are calculated in the framework of the electrostatic model where the polarizabilities of two structural nonequivalent potassium ions are the empirical model parameters. These parameters were fitted using the symmetry of the low-temperature phases. It will be shown that there is a competition between the constants. We believe that such a simple approach enables us to idealize the system under consideration, stressing the basic features of the real crystals, namely, the delicate balance between the interaction constants, which leads to the complex phase diagrams and to remarkable differences among the different members of the
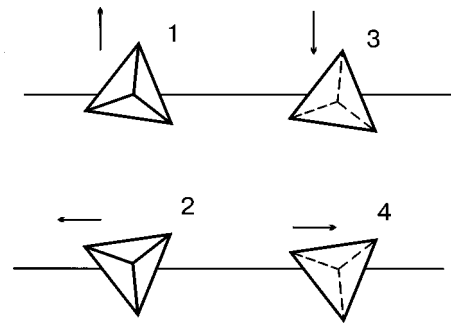
$ACBX_4$ family. The thermodynamical properties of the model are calculated by the Monte Carlo method. Two types of boundary conditions are used: the periodic boundary conditions and the boundary conditions with ''phantom spins.'' It is shown that the model reproduced the experimentally observed sequence of phase transitions including the transition into the modulated phase in K_2SeO_4. The temperature dependence of the modulation vector inside the modulated phase in this compound is also calculated. Since no structural data have been given in the literature on the low-temperature phase in K_2SO_4, except some conflicting suggestions about the space-group symmetry, our theoretical study could be important in resolving the issue.

This paper is organized as follows: In Sec. II we present the model, the method of calculation of the interaction constants, and the results of these calculations. Section III gives the results of the Monte Carlo simulations. A discussion of the results obtained and the comparison with the experimental data can be found in Sec. IV. Section V concludes the paper.

II. MODEL AND CALCULATION OF THE EFFECTIVE INTERACTION CONSTANTS

K_2SO_4 and K_2SeO_4 have hexagonal symmetry with the space group D_{6h}^4 and with two molecules in a unit cell at high temperature. The structure of $ACBX_4$ and its projection viewed down [001] are shown in Fig. 1. The unit cell parameters of both crystals are $a = 5.94$ Å, $c = 8.61$ Å in K_2SO_4, $a = 6.14$ Å, $c = 8.90$ Å in K_2SeO_4.

For calculation of the BX_4-BX_4 interactions and phase diagrams the model proposed in Ref. 12 is used. We take a BX_4 group as a rigid unit which has only the octupole moment and four equilibrium orientations in the disordered hexagonal phase (Fig. 2). The BX_4-BX_4 interaction constants $V_{ij}(R)$ were calculated from the electrostatic model.[13–15] The model used does not explicitly include any displacement of the ions. The effect of these displacements on the energy of the BX_4-BX_4 interactions is included implicitly through the electrostatic dipole interactions of the various sites. The

dipoles are produced by electronic polarizabilities and by displacements of the metals A and C and whole polarizabilities of the metal ions are fitted parameters in the model. Also, the displacements, from the basic hexagonal structure,

$$H = -\frac{1}{2}\sum \mathbf{V}_{oo}^{I,I}(r-r')C_i^I(r)C_j^I(r') - \frac{1}{2}\sum \mathbf{V}_{oo}^{II,II}(r-r')C_i^{II}(r)C_j^{II}(r') - \sum \mathbf{V}_{oo}^{I,II}(r-r')C_i^I(r)C_j^{II}(r')$$

$$+ \sum \mathbf{F}_{od}^{IA}(r-r')C_i^I(r)\mathbf{d}_A(r') + \sum \mathbf{F}_{od}^{IC}(r-r')C_i^I(r)\mathbf{d}_C(r') + \sum \mathbf{F}_{od}^{IIA}(r-r')C_i^{II}(r)\mathbf{d}_A(r')$$

$$+ \sum \mathbf{F}_{od}^{IIC}(r-r')C_i^{II}(r)\mathbf{d}_C(r') + \frac{1}{2\alpha_A}\sum d_A^2(r) + \frac{1}{2\alpha_C}\sum d_C^2(r) + \frac{1}{2}\sum D_{\alpha\beta}^A(r-r')d_\alpha^A(r)d_\beta^A(r')$$

$$+ \frac{1}{2}\sum D_{\alpha\beta}^C(r-r')d_\alpha^C(r)d_\beta^C(r') + \sum D_{\alpha\beta}^{AC}(r-r')d_\alpha^A(r)d_\beta^C(r'), \tag{1}$$

where

$C_i^{I,II} = 1$ if the BX_4 group occupies the position i,

$C_i^{I,II} = 0$ in the   opposite   case,

and the fact that a unit cell of the hexagonal phase has two nonequivalent molecules is taken into account (I and II relate to the sublattices indicated in Fig. 1).

$\mathbf{V}_{oo}^{kl}(r-r')$ is an octupole-octupole interaction matrix, $\mathbf{d}_{A,C}$ a dipole moment of metals A and C which have polarizabilities α_A and α_C. As was mentioned above in the present calculations α_A and α_C are parameters of the theory because they have both electronic and ionic contributions. $\mathbf{D}$ and $\mathbf{F}_{od}$ are, respectively, dipole-dipole and dipole-octupole interaction matrices. In the electrostatic approximation which we used here there is no need to know the magnitudes of the dipole moments of the metal ions, since after elimination of $\mathbf{d}_{A,C}$ from Eq. (1) by standard technique[14,16] we find that, the effective BX_4-BX_4 interaction is a sum of the direct octupole-octupole interaction and the indirect interaction through the polarizable metal ions,

$$\mathbf{H}_{eff} = -\frac{1}{2}\sum \mathbf{V}_{ij}^{I,I}(r-r')C_i^I(r)C_j^I(r') - \frac{1}{2}\sum \mathbf{V}_{ij}^{II,II}(r$$

$$-r')C_i^{II}(r)C_j^{II}(r') - \sum \mathbf{V}_{ij}^{I,II}(r-r')C_i^I(r)C_j^{II}(r'),$$

$$\tag{2}$$

where

$$\mathbf{V}_{ij}^{kl}(r) = \mathbf{V}_{oo}^{kl}(r) + \xi_A\xi_C\mathbf{W}(r), \qquad \xi_{A,C} = \frac{\alpha_{A,C}}{a_0^3},$$

$$\mathbf{W}(r) = \frac{1}{v_0}\int\int\int \mathbf{W}(\mathbf{q})\exp(-i\mathbf{q}\cdot\mathbf{r})d^3\mathbf{q},$$

of the different potassium ions in the unit cell are not simply related to one another, and hence the polarizability values for the different ions are not expected to be the same. The Hamiltonian of the model is

$$\mathbf{W}(\mathbf{q}) = \sum \{J_{\alpha\beta}^A(\mathbf{q})J_{\alpha\beta}^C(\mathbf{q})$$

$$-[D_{\alpha\beta}^{AC}(\mathbf{q})]^2\xi_A\xi_C\}^{-1}\left\{\sum [F_{\alpha n}^A(\omega_1,\mathbf{q})F_{\beta m}^C(\omega_2,\mathbf{q})\right.$$

$$+ F_{\beta m}^A(\omega_2,\mathbf{q})F_{\alpha n}^C(\omega_1,\mathbf{q})]D_{\alpha\beta}^{AC}(\mathbf{q})$$

$$- F_{\alpha n}^A(\omega_1,\mathbf{q})F_{\beta m}^A(\omega_2,\mathbf{q})J_{\alpha\beta}^C(\mathbf{q})/\xi_C$$

$$\left. - F_{\alpha n}^C(\omega_1,\mathbf{q})F_{\beta m}^C(\omega_2,\mathbf{q})J_{\alpha\beta}^A(\mathbf{q})/\xi_A\right\}. \tag{3}$$

$J_{\alpha\beta}^{A,C}(\mathbf{q}) = E_{\alpha\beta} + \xi_{A,C}D_{\alpha\beta}^{A,C}(\mathbf{q})$, $E_{\alpha\beta}$ is a unit matrix, and ω_i are the Euler angles. The interaction matrices $\mathbf{V}^{I,I}$, $\mathbf{V}^{I,II}$, and $\mathbf{V}^{II,II}$ have four independent terms due to the symmetry of the hexagonal phase and the equilibrium orientations (see Figs. 1 and 2):

$$\mathbf{V} = \begin{pmatrix} V_{11} & V_{12} & V_{13} & V_{14} \\ V_{12} & V_{11} & V_{14} & V_{13} \\ V_{13} & V_{14} & V_{11} & V_{12} \\ V_{14} & V_{13} & V_{12} & V_{11} \end{pmatrix}. \tag{4}$$

The interaction tetrahedron BX_4 with five nearest metals of the C type and six nearest metals of the A type is taken into account in the calculations of matrices $\mathbf{F}_{od}$ in Eqs. (3). The matrices $\mathbf{D}$ in Eqs. (3) are calculated by the Ewald method. Integration in $\mathbf{q}$ space was performed by the Gauss method. For K_2SeO_4 the values of polarizabilities were fitted using the symmetry of the ferroelectric low-temperature phase and the region of existence of the incommensurate phase:

$$\alpha_A = 0.60 \text{ Å}^3, \qquad \alpha_C = 0.24 \text{ Å}^3.$$

It should be noted that the use of the values of the electronic polarizabilities of potassium ($\alpha_A = \alpha_C = 0.80$ Å^3) (Ref. 17) leads to a poor agreement with the experimental potassium selenate phase diagram ($D_{6h}^4 \xrightarrow{745 \text{ D}} D_{2h}^{16} \xrightarrow{512 \text{ K}} I \xrightarrow{280 \text{ K}} C_{2v}^9$).

As was mentioned above the symmetry of the low-temperature phase for K_2SO_4 is not clear and in this case the values of the polarizabilities were fitted using the condition that the paraelectric phase (D_{2h}^{16}) exists in a wide temperature region:

$$\alpha_A = 1.2 \ \text{Å}^3, \qquad \alpha_C = 0.14 \ \text{Å}^3.$$

The octupole moment values of the SeO_4 and SO_4 groups, I_3, were fitted using the experimental values of the phase transition ($D_{6h}^4 \to D_{2h}^{16}$) temperatures:

$$I_3(SO_4) = 51.5 \times 10^{-34} \ \text{esu} \ \text{cm}^3,$$

$$I_3(SeO_4) = 51.1 \times 10^{-34} \ \text{esu} \ \text{cm}^3.$$

The effective interaction constants $V_{ij}^{I,I}(R) = V_{ij}^{II,II}(R)$ and $V_{ij}^{I,II}(R)$ were calculated within 19 coordination spheres up to $R = 2c_0$ and their values are presented in Tables I and II. As one can see from these tables, the sign and the magnitude of the interaction constants oscillate as a function of the distance, so that there is a strong competition between the interactions. The result of calculations of the energy at $T = 0$ in the finite system ($16 \times 16 \times 24$) for the phases with the different uniform and nonuniform orderings is shown in Table III. It is seen from the table that there are several phases with the close values of the energies both in K_2SeO_4 and in K_2SO_4. However, there is a difference between them: The phases with the same (potassium sulfate, the phases i and j) and different (potassium selenate, the phases a, c, and h) multiplications of a unit cell have the closest energies. It is this peculiarity of the interactions in K_2SeO_4 that is apparently responsible for the presence of an incommensurate phase at finite temperature.

III. CALCULATION OF THE THERMODYNAMICAL PROPERTIES

The Monte Carlo technique, which is applicable to the Ising-like lattice models,[18,19] is used in the present study. The only change relates to the presence of four equilibrium positions of the BX_4 groups (instead of two positions in the Ising-like models).

The process of determining the thermodynamical values begins with the choice of an initial ''spin'' configuration for a system as a whole. Two initial spin configurations (ordered and disordered) are used for starting Monte Carlo procedure at low temperature and the procedure starts with the last spin configuration generated in the preceding the calculation at the increasing temperature. The program then proceeds through the lattice considering each spin (in order) as the reference spin for trial of turning. One of three positions for turning is chosen randomly. The relative probability of the two states is considered:[19]

$$\rho_{\mu\nu} = \rho_\mu/\rho_\nu = \exp[-(E_\mu - E_\nu)/k_B T]. \tag{5}$$

Equation (5) describes the probability of producing the νth state from the μth one. If $\rho_{\mu\nu} > 1$, the reference spin is turned; otherwise a random number r is chosen from a set of random numbers generated uniformly in the interval from 0 to 1 and compared with $\rho_{\mu\nu}$. If $r < \rho_{\mu\nu}$, the reference spin is

TABLE I. Effective interaction constants, K_2SeO_4.

R	$V_{ij}^{I,II}(\mathbf{R})$ (K)			
	V_{11}	V_{12}	V_{13}	V_{14}
$(a_0^2/3 + c_0^2/4)^{1/2}$	711.5	763.8	−1018.3	−966.1
$(4a_0^2/3 + c_0^2/4)^{1/2}$	95.9	82.8	65.1	52.0
$(7a_0^2/3 + c_0^2/4)^{1/2}$	81.3	79.0	52.8	50.6
$(13a_0^2/3 + c_0^2/4)^{1/2}$	−26.6	−20.2	−30.9	−24.4
$(a_0^2/3 + 9c_0^2/4)^{1/2}$	86.1	79.3	14.7	7.8
$(16a_0^2/3 + c_0^2/4)^{1/2}$	−43.0	−34.7	−41.0	−32.6
$(4a_0^2/3 + 9c_0^2/4)^{1/2}$	−7.0	−3.0	−24.8	−20.8
$(19a_0^2/3 + c_0^2/4)^{1/2}$	−16.4	−18.9	−4.8	−7.4
$(7a_0^2/3 + 9c_0^2/4)^{1/2}$	−14.2	−18.1	−18.0	−21.9

R	$V_{ij}^{I,I}(\mathbf{R}) = V_{ij}^{II,II}(\mathbf{R})$ (K)			
	V_{11}	V_{12}	V_{13}	V_{14}
a_0	571.8	603.9	−489.9	−457.8
c_0	−11.7	−4.4	53.0	60.3
$a_0\sqrt{3}$	16.8	16.5	−13.5	−13.7
$(a_0^2 + c_0^2)^{1/2}$	13.4	2.8	47.5	36.9
$2a_0$	3.9	3.6	−7.7	−7.9
$(3a_0^2 + c_0^2)^{1/2}$	3.7	3.4	−1.2	−1.5
$(4a_0^2 + c_0^2)^{1/2}$	1.4	1.4	−1.0	−1.0
$a_0\sqrt{7}$	−2.2	−2.7	2.1	1.6
$2c_0$	8.6	7.4	−27.2	−28.4

TABLE II. Effective interaction constants, K_2SO_4.

R	$V_{ij}^{I,II}(\mathbf{R})$ (K)			
	V_{11}	V_{12}	V_{13}	V_{14}
$(a_0^2/3+c_0^2/4)^{1/2}$	793.5	839.4	−1126.7	−1080.9
$(4a_0^2/3+c_0^2/4)^{1/2}$	89.2	83.3	147.0	141.1
$(7a_0^2/3+c_0^2/4)^{1/2}$	90.1	66.8	93.2	70.0
$(13a_0^2/3+c_0^2/4)^{1/2}$	−31.1	−26.5	−42.5	−37.9
$(a_0^2/3+9c_0^2/4)^{1/2}$	147.8	144.7	10.6	7.5
$(16a_0^2/3+c_0^2/4)^{1/2}$	−50.0	−45.6	−60.6	−56.3
$(4a_0^2/3+9c_0^2/4)^{1/2}$	3.7	5.6	−18.1	−16.1
$(19a_0^2/3+c_0^2/4)^{1/2}$	−22.5	−14.9	−5.4	2.3
$(7a_0^2/3+9c_0^2/4)^{1/2}$	−14.1	−13.4	−14.2	−13.6

R	$V_{ij}^{I,I}(\mathbf{R})=V_{ij}^{II,II}(\mathbf{R})$ (K)			
	V_{11}	V_{12}	V_{13}	V_{14}
a_0	623.4	622.6	−575.2	−576.0
c_0	32.3	39.3	103.4	110.4
$a_0\sqrt{3}$	15.7	14.9	−10.9	−11.7
$(a_0^2+c_0^2)^{1/2}$	28.0	11.5	135.7	119.2
$2a_0$	−0.7	−0.9	−8.1	−8.2
$(3a_0^2+c_0^2)^{1/2}$	4.4	3.9	3.2	2.8
$(4a_0^2+c_0^2)^{1/2}$	0.9	0.9	0.7	0.8
$a_0\sqrt{7}$	−4.0	−4.6	2.8	2.2
$2c_0$	3.9	2.9	−61.0	−62.0

turned. E_μ and E_ν in Eq. (5) are energies of the states μ and ν. In the present work two types of boundary conditions are used: the periodic conditions and the boundary conditions with ''phantom spins.'' The latter were recently proposed in Ref. 20 for investigation of systems with competing interactions. In Ref. 20 the two-dimensional X-Y model was studied by the Monte Carlo method. In the present work the boundary conditions with phantoms are somewhat modified in comparison with those in Ref. 20 since here a discrete pseudospin, instead of the continuous one in the X-Y model, occupies each lattice site. The changes concern the configuration of the phantom spins surrounding the main spins. The number of the phantoms is determined by the number of the interacting coordination spheres, and their configuration after each Monte Carlo step is set according to the obtained configuration of the main lattice.

It should be noted that we tried the free boundary conditions, but in the our case, even at low temperatures, the system very rapidly slid into a metastable state and remained in it with a reasonable number of Monte Carlo steps. This is associated with the fact that, even for a lattice of quite large size, too many spins remain free because there is a great number of interactions and the competition between them makes the system very unstable.

The calculations are carried out on the $N\times N\times N1$ hexagonal three-dimensional lattice. Two sizes of lattice ($N=16$, $N1=24$ and $N=24$, $N1=48$) are treated here. As is seen from Figs. 3 and 4 the results of the Monte Carlo calculations are close to each other for different lattice sizes and below we will discuss the results of the calculations only for the lattice with $N=24$ and $N1=48$.

The thermodynamical quantities were calculated in the usual way,[18,19]

$$U=\sum_{m=1}^{N}\sum_{s=1}^{18} V_{ij}(s,m),$$

$$C=\frac{N^2}{kT^2}(\Delta U)^2,$$

$$\chi_i=\frac{N^2}{kT}(\Delta \eta_i)^2, \tag{6}$$

where U is the internal energy, C is the heat capacity, η_i are the order parameters which will be determined below, χ_i is susceptibility, and $(\Delta A)^2=\langle A^2\rangle-\langle A\rangle^2$.

One Monte Carlo (MC) step per spin was $N\times N\times N1$ spin turning trials. The first 500–1000 MC steps were discarded and not used in computing averages. Averaging was carried out in two steps: After p MC steps subaverages were determined for the group of states (usually $p=50$), and then after a number of subaverages (usually 85) the final averages were computed. The calculations were repeated at another temperature and so on.

The program, written in FORTRAN, required about 0.2 msec per spin on a Pentium/60 computer.

The structures of the ordered phases which resulted from Monte Carlo simulations at low temperature have the following occupation numbers (n_i corresponds to the i orientation of a tetrahedron in Fig. 2):

TABLE III. Energies and structures of the ordered low-temperature phases. The directions of arrows correspond to the orientations of the BX_4 tetrahedron in Fig. 2. The digit in the second line indicates the number of the layer along the pseudohexagonal axis. The phase a, ferroelectric one in K_2SeO_4 $[C_{2v}^9(z=12)]$, and the phase i, low-temperature phase in K_2SO_4 $[C_{2h}^5(z=16)]$.

	Structures of the ordered phases												Energy (K)	
	1		2		3		4		5		6		KSe	KS
a	↑	↓	↓	↑	↑	↓	→	←	←	→	→	←	−1225	−904
	↓	↑	↑	↓	↓	↑	←	→	→	←	←	→		
b	←	→	↓	↑	↑	↓	↓	↑	←	→	→	←	−1083	−867
	↑	↓	→	←	→	←	←	→	↑	↓	↓	↑		
c	↑	↓	↓	↑	↑	↓	↓	↑	↑	↓	↓	↑	−1206	−863
	↑	↓	↓	↑	↑	↓	↓	↑	↑	↓	↓	↑		
d	←	←	↓	↓	↑	↑	↓	↓	←	←	→	→	−1163	−870
	←	←	↓	↓	↑	↑	↓	↓	←	←	→	→		
e	↑	↑	↓	↓	↑	↑	↓	↓	↑	↑	↓	↓	−1146	−829
	↑	↑	↓	↓	↑	↑	↓	↓	↑	↑	↓	↓		
f	→	↑	←	↓	→	↑	←	↓	→	↑	←	↓	−1148	−913
	↑	→	↓	←	↑	→	↓	←	↑	→	↓	←		

	1				2				3					
g	←	←	→	→	→	→	←	←	←	←	→	→	−1208	−899
	→	→	←	←	←	←	→	→	→	→	←	←		

	4				5				6					
	→	→	←	←	←	←	→	→	→	→	←	←		
	←	←	→	→	→	→	←	←	←	←	→	→		

	1				2				3					
h	↑	↑	↓	↓	↓	↓	↑	↑	↑	↑	↓	↓	−1150	−948
	→	→	←	←	←	←	→	→	→	→	←	←		

	4				5				6					
	↓	↓	↑	↑	↑	↑	↓	↓	↓	↓	↑	↑		
	←	←	→	→	→	→	←	←	←	←	→	→		

	1				2				3					
i	↑	↑	←	←	↓	↓	→	→	↑	↑	←	←	−1185	−949
	→	→	↓	↓	←	←	↑	↑	→	→	↓	↓		

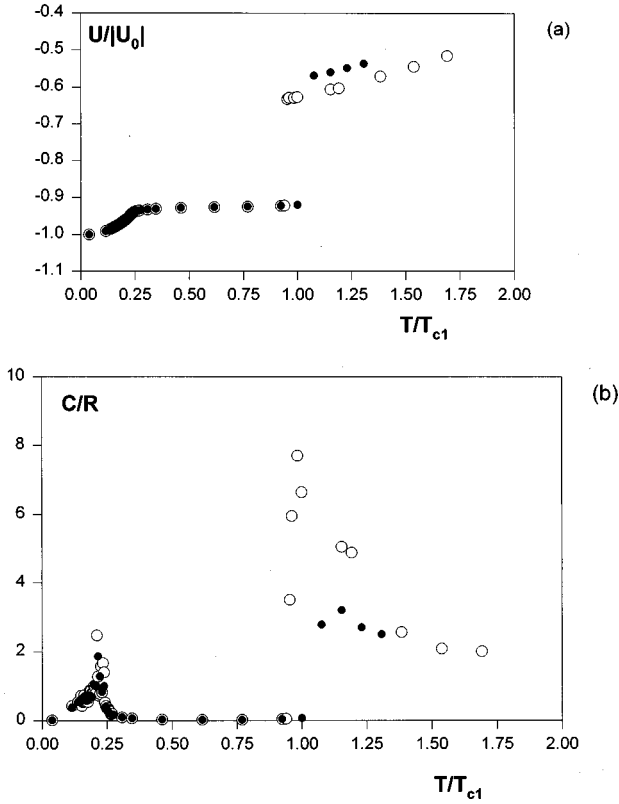|	4				5				6					
	↓	↓	→	→	↑	↑	←	←	↓	↓	→	→		
	←	←	↑	↑	→	→	↓	↓	←	←	↑	↑		

FIG. 3. The temperature dependence of internal energy (a) and specific heat (b) for K_2SeO_4. The open and solid circles: the results for the lattices $24\times24\times48$ and $16\times16\times24$, respectively.

For K_2SeO_4,

$$n_1^I(\mathbf{R}_0)=n_3^I(\mathbf{R}_1)=n_1^{II}(\mathbf{R}_7)=n_3^{II}(\mathbf{R}_6)=1,$$

$$n_1^I(\mathbf{R}_2)=n_3^I(\mathbf{R}_3)=n_2^{II}(\mathbf{R}_8)=n_4^{II}(\mathbf{R}_9)=1,$$

$$n_2^I(\mathbf{R}_4)=n_4^I(\mathbf{R}_5)=n_2^{II}(\mathbf{R}_{10})=n_4^{II}(\mathbf{R}_{11})=1, \qquad (7)$$

where

$$\mathbf{R}_0=(0,0,0), \quad \mathbf{R}_6=\left(-\frac{1}{2\sqrt{3}}a_0,\frac{a_0}{2},\frac{c_0}{2}\right),$$

$$\mathbf{R}_1=\left(\frac{\sqrt{3}}{2}a_0,-\frac{a_0}{2},0\right), \quad \mathbf{R}_7=\left(\frac{1}{\sqrt{3}}a_0,a_0,\frac{c_0}{2}\right),$$

$$\mathbf{R}_2=(0,0,c_0), \quad \mathbf{R}_8=\left(-\frac{1}{2\sqrt{3}}a_0,\frac{a_0}{2},\frac{3c_0}{2}\right),$$

$$\mathbf{R}_3=\left(\frac{\sqrt{3}}{2}a_0,-\frac{a_0}{2},c_0\right), \quad \mathbf{R}_9=\left(\frac{1}{\sqrt{3}}a_0,a_0,\frac{3c_0}{2}\right),$$

$$\mathbf{R}_4=(0,0,2c_0), \quad \mathbf{R}_{10}=\left(-\frac{1}{2\sqrt{3}}a_0,\frac{a_0}{2},\frac{5c_0}{2}\right),$$

$$\mathbf{R}_5=\left(\frac{\sqrt{3}}{2}a_0,-\frac{a_0}{2},2c_0\right), \quad \mathbf{R}_{11}=\left(\frac{1}{\sqrt{3}}a_0,a_0,\frac{5c_0}{2}\right).$$
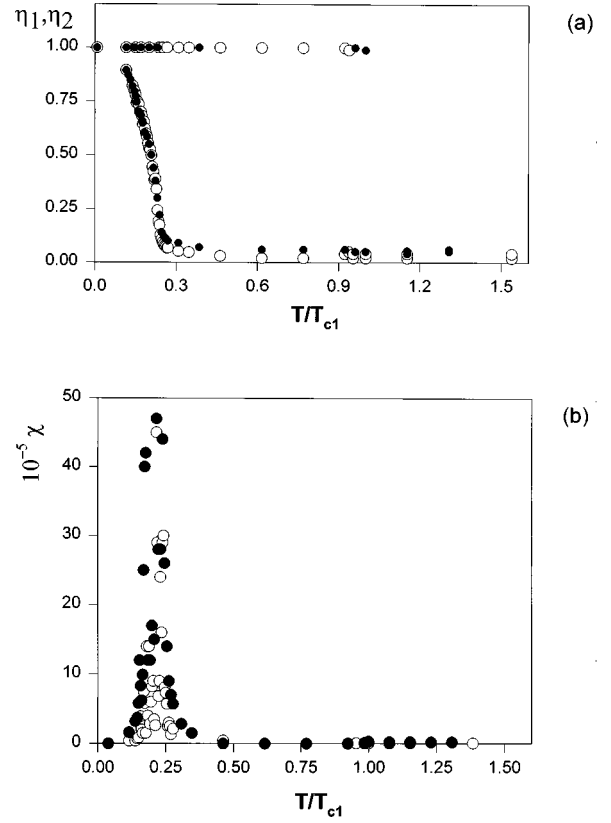
FIG. 4. The temperature dependences of order parameters η_1 and η_2 (a) and susceptibility (b) for K_2SeO_2. The notation is the same as in Fig. 3.

The ordered phase has the orthorhombic symmetry with the polar space group C_{2v}^9 and 12 molecules per unit cell.

For K_2SO_4,

$$n_1^I(\mathbf{R}_0)=n_4^I(\mathbf{R}_1)=n_1^{II}(\mathbf{R}_8)=n_4^{II}(\mathbf{R}_6)=1,$$

$$n_1^I(\mathbf{R}_2)=n_4^I(\mathbf{R}_5)=n_1^{II}(\mathbf{R}_7)=n_4^{II}(\mathbf{R}_{13})=1,$$

$$n_2^I(\mathbf{R}_3)=n_3^I(\mathbf{R}_{12})=n_2^{II}(\mathbf{R}_{10})=n_3^{II}(\mathbf{R}_{14})=1,$$

$$n_2^I(\mathbf{R}_4)=n_3^I(\mathbf{R}_9)=n_2^{II}(\mathbf{R}_{11})=n_3^{II}(\mathbf{R}_{15})=1, \qquad (8)$$

where

$$\mathbf{R}_0=(0,0,0), \quad \mathbf{R}_8=\left(\frac{1}{\sqrt{3}}a_0,0,\frac{c_0}{2}\right),$$

$$\mathbf{R}_1=\left(\frac{\sqrt{3}}{2}a_0,-\frac{a_0}{2},0\right), \quad \mathbf{R}_7=\left(\frac{1}{\sqrt{3}}a_0,a_0,\frac{c_0}{2}\right),$$

$$\mathbf{R}_2=(0,a_0,0), \quad \mathbf{R}_{10}=\left(\frac{1}{\sqrt{3}}a_0,2a_0,\frac{c_0}{2}\right),$$

$$\mathbf{R}_3=(0,2a_0,0), \quad \mathbf{R}_{11}=\left(\frac{1}{\sqrt{3}}a_0,3a_0,\frac{c_0}{2}\right),$$

$$\mathbf{R}_4 = (0, 3a_0, 0), \qquad \mathbf{R}_6 = \left(-\frac{1}{2\sqrt{3}}a_0, \frac{a_0}{2}, \frac{c_0}{2} \right),$$

$$\mathbf{R}_5 = \left(\frac{\sqrt{3}}{2}a_0, \frac{a_0}{2}, 0 \right), \qquad \mathbf{R}_{13} = \left(-\frac{1}{2\sqrt{3}}a_0, \frac{3a_0}{2}, \frac{c_0}{2} \right),$$

$$\mathbf{R}_{12} = \left(\frac{\sqrt{3}}{2}a_0, \frac{3a_0}{2}, 0 \right), \qquad \mathbf{R}_{14} = \left(-\frac{1}{2\sqrt{3}}a_0, \frac{5a_0}{2}, \frac{c_0}{2} \right),$$

$$\mathbf{R}_9 = \left(\frac{\sqrt{3}}{2}a_0, \frac{5a_0}{2}, 0 \right), \qquad \mathbf{R}_{15} = \left(-\frac{1}{2\sqrt{3}}a_0, \frac{7a_0}{2}, \frac{c_0}{2} \right).$$

The ordered phase has monoclinic symmetry with the nonpolar space group C_{2h}^5 and 16 molecules per unit cell. The values of $n_i^k(R)$ were determined from the Monte Carlo data at the temperature $T/T_{c1} = 0.08$, where T_{c1} is the temperature of the hexagonal-orthorhombic phase transition. At lower temperatures the problem of metastable states arises when the system cools from the disordered or modulated phases. The order parameters (η_1, η_2, η_3) are written in terms of the occupation numbers $n_i^{I,II}$ as follows.

The order parameter common for K_2SeO_4 and K_2SO_4 is

$$\eta_1 = \frac{1}{4}\{[n_1^I(\mathbf{R}_0) + n_2^I(\mathbf{R}_0) - n_3^I(\mathbf{R}_0) - n_4^I(\mathbf{R}_0) + n_3^I(\mathbf{R}_1)$$
$$+ n_4^I(\mathbf{R}_1) - n_1^I(\mathbf{R}_1) - n_2^I(\mathbf{R}_1)] + [n_3^{II}(\mathbf{R}_6) + n_4^{II}(\mathbf{R}_6)$$
$$- n_1^{II}(\mathbf{R}_6) - n_2^{II}(\mathbf{R}_6) + n_1^{II}(\mathbf{R}_7) + n_2^{II}(\mathbf{R}_7) - n_3^{II}(\mathbf{R}_7)$$
$$- n_4^{II}(\mathbf{R}_7)]\}. \tag{9}$$

The order parameter η_2 for K_2SeO_4 is

$$\eta_2 = \frac{1}{12}\left\{ \sum_{\mathbf{R}=\mathbf{R}_0, \mathbf{R}_1, \mathbf{R}_2, \mathbf{R}_3} [n_1^I(\mathbf{R}) - n_2^I(\mathbf{R}) + n_3^I(\mathbf{R}) - n_4^I(\mathbf{R})] \right.$$

$$+ \sum_{\mathbf{R}=\mathbf{R}_7, \mathbf{R}_6} [n_1^{II}(\mathbf{R}) - n_2^{II}(\mathbf{R}) + n_3^{II}(\mathbf{R}) - n_4^{II}(\mathbf{R})]$$

$$+ \sum_{\mathbf{R}=\mathbf{R}_4, \mathbf{R}_5} [n_2^I(\mathbf{R}) - n_1^I(\mathbf{R}) + n_4^I(\mathbf{R}) - n_3^I(\mathbf{R})]$$

$$+ \sum_{\mathbf{R}=\mathbf{R}_8, \mathbf{R}_9, \mathbf{R}_{10}, \mathbf{R}_{11}} \left. [n_2^{II}(\mathbf{R}) - n_1^{II}(\mathbf{R}) + n_4^{II}(\mathbf{R}) - n_3^{II}(\mathbf{R})] \right\}. \tag{10}$$

The order parameter η_3 for K_2SO_4 is

$$\eta_3 = \frac{1}{16}\left\{ \sum_{\mathbf{R}=\mathbf{R}_0, \mathbf{R}_1, \mathbf{R}_2, \mathbf{R}_5} [n_1^I(\mathbf{R}) - n_2^I(\mathbf{R}) + n_4^I(\mathbf{R}) - n_3^I(\mathbf{R})] \right.$$

$$+ \sum_{\mathbf{R}=\mathbf{R}_8, \mathbf{R}_7, \mathbf{R}_6, \mathbf{R}_{13}} [n_1^{II}(\mathbf{R}) - n_2^{II}(\mathbf{R}) + n_4^{II}(\mathbf{R}) - n_3^{II}(\mathbf{R})]$$

$$+ \sum_{\mathbf{R}=\mathbf{R}_3, \mathbf{R}_4, \mathbf{R}_{12}, \mathbf{R}_9} [n_2^I(\mathbf{R}) - n_1^I(\mathbf{R}) + n_3^I(\mathbf{R}) - n_4^I(\mathbf{R})]$$

$$+ \sum_{\mathbf{R}=\mathbf{R}_{10}, \mathbf{R}_{11}, \mathbf{R}_{14}, \mathbf{R}_{15}} [n_2^{II}(\mathbf{R}) - n_1^{II}(\mathbf{R}) + n_3^{II}(\mathbf{R})$$

$$\left. - n_4^{II}(\mathbf{R})] \right\}, \tag{11}$$

where the equivalence of unit cell parameters a_0 and b_0 in the hexagonal phase is taken into account. The results of the calculations of the thermodynamical quantities are presented in Figs. 3–7. The typical error bars near the critical points and far from the critical points are 10% and 3%, respectively.

There are three in K_2SeO_4 and two in K_2SO_4 successive phase transitions. The first of them occurs in both crystals, when the temperature decreases and is caused by the partial ordering of the BX_4 tetrahedra. The partially ordered phase is described by the following occupation numbers (when η_1 is equal to 1):

$$n_1^I(R=0) = n_2^I(R=0) = n_3^I(R=a_0) = n_4^I(R=a_0) = \frac{1}{2},$$

$$n_3^I(R=0) = n_4^I(R=0) = n_1^I(R=a_0) = n_2^I(R=a_0) = 0,$$

$$n_3^{II}(R=b_0) = n_4^{II}(R=b_0) = n_1^{II}(R=c_0) = n_2^{II}(R=c_0) = \frac{1}{2},$$

$$n_1^{II}(R=b_0) = n_2^{II}(R=b_0) = n_3^{II}(R=c_0) = n_4^{II}(R=c_0) = 0. \tag{12}$$

The symmetry of the partially ordered phase is orthorhombic with the space group D_{2h}^{16} and with four molecules in a unit cell. This phase transition is observed experimentally at high temperatures in both crystals under consideration.[4,5] The temperature dependences of the internal energy, the order parameter η_1, heat capacity, and susceptibility χ_1 at the phase transition from the hexagonal phase to the orthorhombic one are shown in Figs. 3–6.

In the case of K_2SO_4 as the temperature decreases further, the second phase transition caused by the full ordering of the SO_4 groups occurs. This ordered phase is a monoclinic one with the space group C_{2h}^5 and with 16 molecules in the unit cell. The calculated temperature of this transition is 75 K. The behavior of the internal energy and the specific heat at this transition is shown in Fig. 5. The $D_{2h}^{16} \rightarrow C_{2h}^5$ phase transition is not observed experimentally in K_2SO_4, but from the results of the specific heat measurements it was suggested[7] that K_2SO_4 might undergo a phase transition at 56 K.

In the case of K_2SeO_4 as the crystal is cooled further, a phase transition into the modulated phase occurs at $T_i = 170$ K. The experimental value of T_i is 130 K.[6] Finally, at $T_{c2} = 115$ K a lock-in transition into a ferroelectric ordered
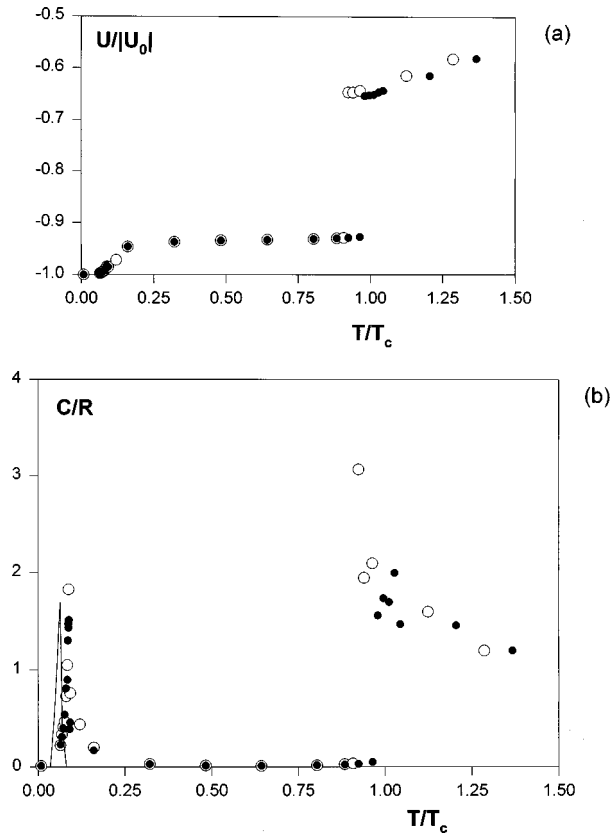
FIG. 5. The temperature dependence of internal energy (a) and specific heat (b) for K_2SO_4. The notation is the same as in Fig. 3. The solid line represents the experimental data of Ref. 7.

FIG. 6. The temperature dependence of the specific heat for K_2SeO_4 (size of the lattice is $24 \times 24 \times 48$). The solid and open circles: the periodic boundary conditions and conditions with phantoms, respectively. The solid line represents the experimental data of Ref. 6.

phase with the space group C_{2v}^9 and 12 molecules per unit cell takes place. The pseudohexagonal axis is tripled compared to that in the paraelectric phase, as is observed experimentally at $T_{c2}^{expt} = 95$ K.[6]

The phase transition temperatures in the crystals under consideration, excluding the lock-in transition temperature in potassium selenate, were determined from the peaks in the temperature dependence of the specific heat (Figs. 5 and 6). In the case of K_2SeO_4 we have met the difficulties in determining the temperature T_{c2} of the lock-in transition into the commensurate ferroelectric phase from the Monte Carlo calculations of the specific heat in the case of K_2SeO_4 due to the considerable scatter of the specific heat inside the incommensurate phase (see Figs. 3 and 6). The temperature of the lock-in transition is estimated from the inflection in the temperature dependence of the internal energy (Fig. 3). It should be noted that the values of the phase transition temperatures T_{c1}, T_{c2} (for both crystals), and T_i (for potassium selenate) calculated with the boundary conditions with phantom spins and with periodic boundary conditions are close.

Let us discuss the incommensurate phase in K_2SeO_4. The structure of this phase is spatially modulated along the pseudohexagonal axis and the modulation depends on the temperature. According to the Monte Carlo data the ordering of the SeO_4 tetrahedra in layers perpendicular to the pseudohexagonal axis is uniform at all temperatures including the region in which the modulated phase exists. However, inside this phase the degree of the tetrahedra ordering changes from layer to layer. Figure 8 displays the degree of
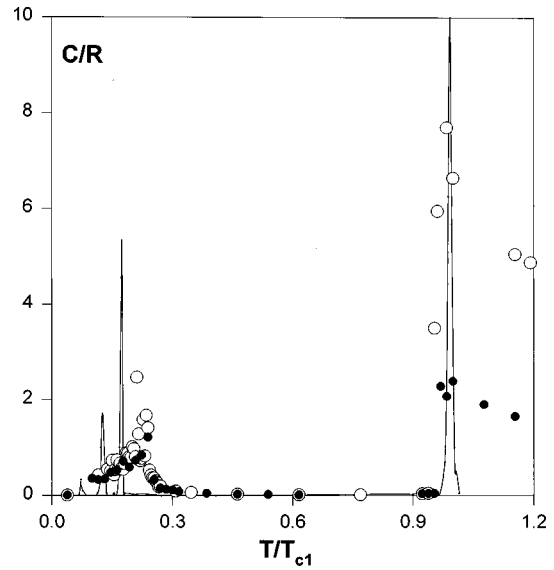
the tetrahedra ordering in the layers for two temperatures inside the modulated phase. The ordering inside the layers in the ordered ferroelectric phase is shown in Fig. 8 for comparison. The long-wavelength modulation inside the incommensurate phase depends on the temperature. This is especially noticeable when phantom spins are used in the boundary conditions. In this case the system itself selects the modulation period. This dependence is less strong in the case of the periodic boundary conditions due to the fact that the conditions impose a specific period on the system at all temperatures. One can see from Fig. 8 that there is the short-wavelength modulation in addition to the long-wavelength one inside the incommensurate phase. The period of this modulation is $3 \times c_0$; i.e., it is the unit cell parameter of the ferroelectric phase. Here, there is a great difference in the average magnitude of the orientations of the SeO_4 tetrahedra from layer to layer along with the different orientations in the layers.

To determine the temperature dependence of the modulation period we calculated the structure factor $S(\mathbf{q})$ in terms of the correlation function $G_{11}(\mathbf{R})$:

$$S(\mathbf{q}) = \sum_{\mathbf{R}} G_{11}(\mathbf{R}) \exp(i\mathbf{q} \cdot \mathbf{R}),$$

$$G_{11}(\mathbf{R}) = \sum_{i=1}^{N \times N \times N_1} C_1(\mathbf{r}_i) C_1(\mathbf{r}_i - \mathbf{R}). \quad (13)$$

The function $S(2,0,q_z)$ for the different temperatures is displayed in Fig. 9. One can see that in the ferroelectric phase, in addition to the peak at $q=0$, there is a peak at $q=1/3$. We would like to note that the same peak appears at all 1/3-fold q as well. Inside the modulated phase the position of this peak varies slightly with the temperature, but with the tem-
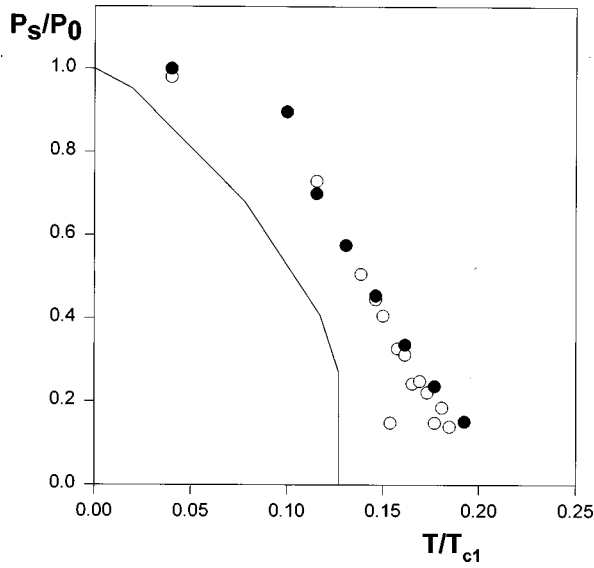
FIG. 7. The temperature dependence of the spontaneous polarization for K_2SeO_4. The notation is the same as in Fig. 6. The experimental data are from Ref. 21.

perature increase the intensity of the peak decreases strongly and the peak vanishes when the system is in the paraelectric phase.

For K_2SO_4 the functions $S(\mathbf{q}_1)$ and $S(\mathbf{q}_2)$ were calculated (Fig. 10). Here, in addition to the peak at $q=0$, there are peaks at $q=\frac{1}{2}b_0^*$ along $\mathbf{q}_1=(q,0,0)$ and $q=\frac{1}{4}a_0^*$ along $\mathbf{q}_2=((\sqrt{3}/2)q,\frac{1}{2}q,0)$ in the low-temperature phase and positions of the peaks do not vary with temperature.

IV. DISCUSSION: COMPARISON WITH EXPERIMENT

The temperature dependences of the internal energy, the specific heat, the order parameters, and susceptibilities, as obtained from Monte Carlo data for two types of boundary conditions, are shown in Figs. 3–7. The solid curve in Figs. 5 and 6 represents the experimental data on the specific heat of potassium selenate and sulphate.[6,7] It is seen from these figures that there is a satisfactory agreement between computed and experimental dependences, excluding the region in which the modulated phase exists. In this region the Monte Carlo calculations give a considerable spread in the specific heat, as was mentioned above. K_2SeO_4 is nonintrinsic ferroelectric material and therefore the measured parameter is the spontaneous polarization P_s. In investigating the model we
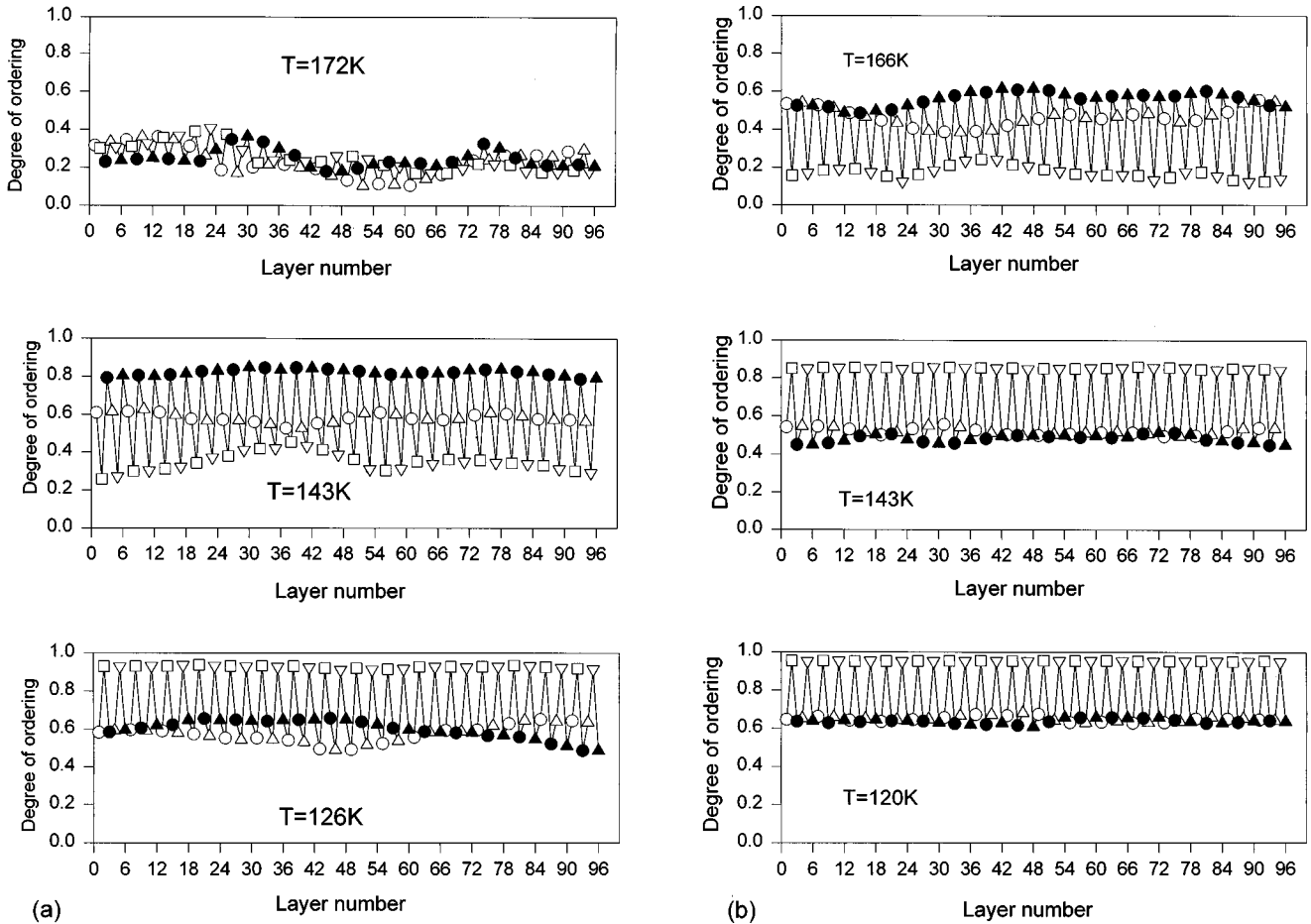

FIG. 8. The spatial dependence of the degree of order in layers for K_2SeO_4. Open and solid circles, the ordering of $\uparrow\downarrow\uparrow\downarrow$, $\downarrow\uparrow\downarrow\uparrow$; open and solid triangles, the ordering of $\rightarrow\leftarrow\rightarrow\leftarrow$, $\leftarrow\rightarrow\leftarrow\rightarrow$; open squares, the ordering of $\downarrow\uparrow\downarrow\uparrow$, $\uparrow\downarrow\uparrow\downarrow$; open and solid triangles, the ordering of $\leftarrow\rightarrow\leftarrow\rightarrow$, $\rightarrow\leftarrow\rightarrow\leftarrow$. (a) Boundary conditions with phantom spins. (b) Periodic boundary conditions.
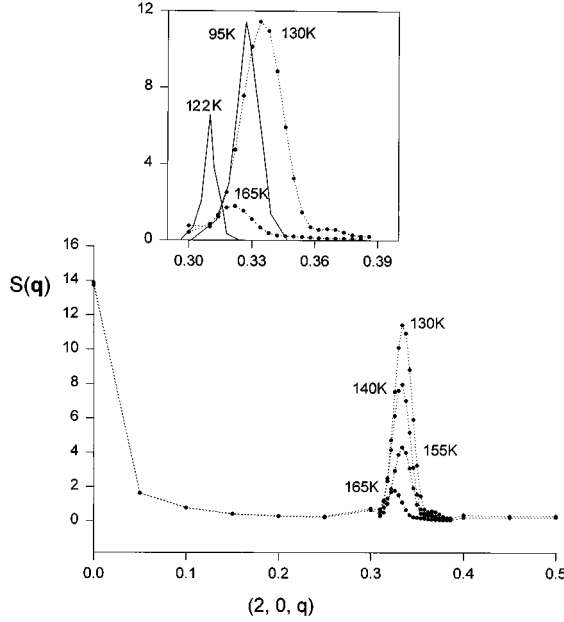
FIG. 9. Structure factor as a function of the wave vector at different temperatures in K_2SeO_4. Inset: profile of the x-ray reflection of the first satellite with q. The dashed curves represent the Monte Carlo data (phantom spins boundary condition) and the solid curves represent the experimental data from Ref. 23.

found that the ordering of the SeO_4 tetrahedra corresponded to the polar group C_{2v}^9 at low temperatures and due to this the spontaneous polarization could occur at the phase transition into this phase as the secondary order parameter. The absolute value of P_s in the ferroelectric phase we could not calculate, since the displacement of the metal atoms and distortion of the BX_4 tetrahedra in the low-symmetry phase were not taken into account explicitly in the model. But the temperature dependence of P_s can be found. The parameter P, defined in terms of $n_i^{I,II}$ as
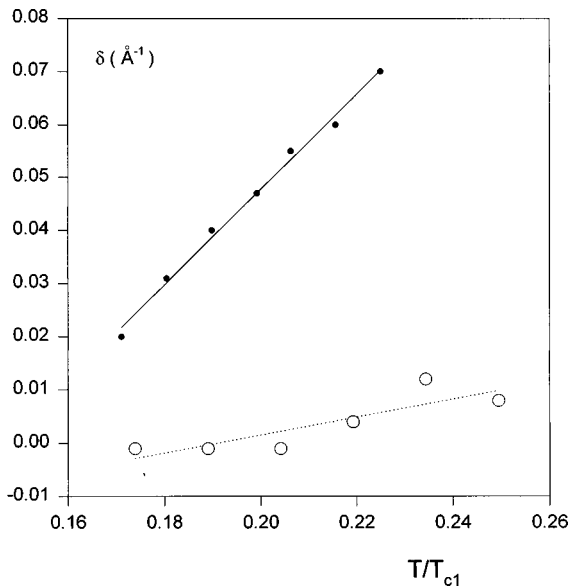

FIG. 10. The temperature dependence of the vector δ in K_2SeO_4. The open circles represent the Monte Carlo data (phantom spins boundary condition) and the points represent the experimental data from Ref. 23.
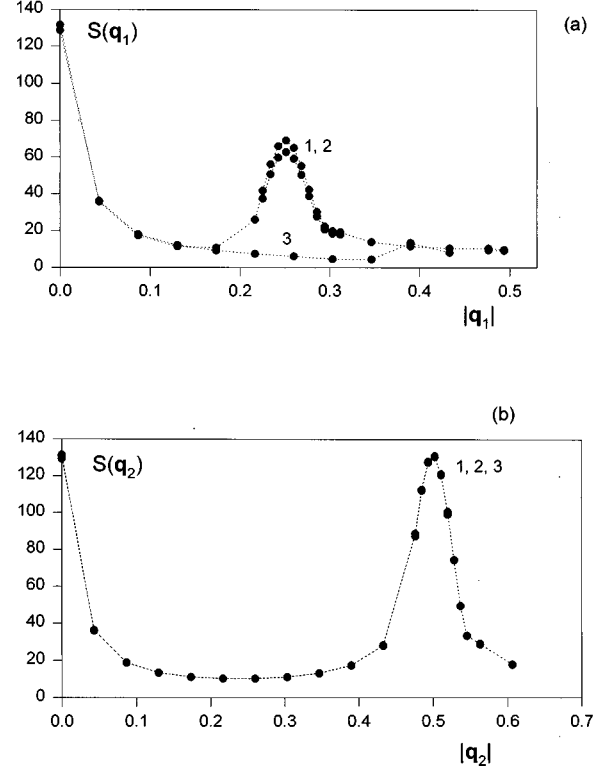

FIG. 11. Structure factor as a function of the wave factor at different temperatures (1–55 K, 2–70 K, and 3–90 K) in K_2SO_4: (a) along $\mathbf{a}_0^*$ and (b) along $\mathbf{b}_0^*$.

$$
\begin{aligned}
P_s = \frac{1}{4} \{ & n_1^I(\mathbf{R}_0) - n_2^I(\mathbf{R}_0) + n_3^I(\mathbf{R}_0) - n_4^I(\mathbf{R}_0) + n_1^{II}(\mathbf{R}_6) \\
& - n_2^{II}(\mathbf{R}_6) + n_3^{II}(\mathbf{R}_6) - n_4^{II}(\mathbf{R}_6) + n_2^I(\mathbf{R}_1) - n_1^I(\mathbf{R}_1) \\
& + n_4^I(\mathbf{R}_1) - n_3^I(\mathbf{R}_1) + n_2^{II}(\mathbf{R}_7) - n_1^{II}(\mathbf{R}_7) + n_4^{II}(\mathbf{R}_7) \\
& - n_3^{II}(\mathbf{R}_7) \},
\end{aligned}
\tag{14}
$$

transforms under the symmetry operation in the same manner as P_s and thus it is proportional to the spontaneous polarization. The computed and experimental temperature dependences of the polarization of potassium selenate are shown in Fig. 7, and they are in good agreement.

The structure of the modulated phase of the potassium selenate was determined in Refs. 22 and 23. It was found that the modulation of the structure was determined mainly by the nonuniform (in the direction of the pseudohexagonal axis) rotation of the SeO_4 tetrahedra, and it was of long-wavelength character. The long-wavelength modulation computed here agrees qualitatively with the experimental one. But the short-wavelength modulation found here from the Monte Carlo simulation was not observed experimentally. The temperature dependence of the modulation vector in the incommensurate phase of K_2SeO_4 was found from the temperature dependence of the x-ray reflection on the vector $(2,0,q_z)$. The experimental and Monte Carlo values of the x-ray reflection intensities at different temperatures inside the modulated phase are shown in Fig. 9. Figure 11 displays the temperature dependence of δ. As one can see from these

figures there is only a qualitative agreement between the computed and experimental curves. The experimental curve of the intensity is more narrow than the computed one, and the measured maximum value of δ is almost 3 times higher than that obtained from the Monte Carlo data.

V. CONCLUSION

Let us summarize the basic results obtained in this work. We have applied the Monte Carlo method to study the order-disorder phase transitions in K_2SeO_4 and K_2SO_4. The effective constants of interactions between SeO_4 (SO_4) groups were calculated in the framework of the electrostatic approximation, where the polarizabilities of potassium ions are taken as fitted parameters. The phase diagrams are sensitive to the values of the polarizabilities. As was mentioned above the use of the calculated value for the electronic polarizability of K^+ [$\alpha_K = 0.8$ Å^3 (Ref. 17)] leads to the poor agreement between the calculated and experimental phase transition temperatures for K_2SeO_4 and to the difference between the calculated and experimental phase diagrams for K_2SO_4. Apparently it means that the role of the ionic contribution to the K^+ polarizability is important for describing the phase transition in the crystals. In our study the values of the polarizabilities of the structural nonequivalent potassium ions in K_2SeO_4 and K_2SO_4 are strongly different. As is seen from Fig. 1, these ions have different coordination polyhedra and, apparently, this fact leads to the difference in the polar-

izability values. The results obtained show that the treatment of the model by the Monte Carlo method yields a correct description of the sequence of the transitions in these crystals, including the intermediate modulated phase in potassium selenate. The strong difference between the phase diagrams of the potassium selenate and potassium sulphate is caused by the delicate balance of the competing interaction constants. The reason for the difference in the fitted parameters α_K in these crystals is not clear to us, and we can only suppose that it is associated with the different sizes of the SO_4 and SeO_4 tetrahedra: Apparently, the elastic contribution into the polarizability of the potassium ion in K_2SO_4 is higher than that in K_2SeO_4, since the size of SO_4 is less than that of SeO_4. The computed temperatures T_i and T_{c2} and the behavior of the thermodynamic parameters are in a satisfactory agreement with the experimental data.

The results of the investigation of the model allow us to predict the group of symmetry of the low-temperature phase in potassium sulphate and the existence of a short-wavelength modulation in the modulated phase of potassium selenate. It would be interesting to have experimental verification of these predictions.

[1] K. S. Aleksandrov and B. V. Beznosikov, *Structural Phase Transitions in Crystals (Potassium Selenate Family)* (Nauka, Novosiborsk, 1993).

[2] H. Z. Cummins, Phys. Rep. **185**, 211 (1990).

[3] W. Eysel, Ph.D. thesis, Achen University, 1975.

[4] H. Arnold, W. Kurtz, A. Richter-Zinnius, and J. Bethke, Acta Crystallogr., Sect. B: Struct. Crystallogr. Cryst. Chem. **37**, 1643 (1981).

[5] K. Inoue, K. Suzuki, A. Sawada, Y. Ishibashi, and Y. Takagi, J. Phys. Soc. Jpn. **46**, 608 (1979).

[6] A. Lopez Echarri, M. J. Tello, and P. Gili, Solid State Commun. **36**, 1021 (1980).

[7] K. Gesi, Y. Tominaga, and H. Urabe, Ferroelectr. Lett. **44**, 71 (1982).

[8] M. Scrocco, Phys. Status Solidi B **91**, K21 (1979).

[9] K. Ojima, Y. Nishihata, and A. Sawada, Acta Crystallogr., Sect. B: Struct. Sci. **51**, 287 (1995).

[10] H. M. Lu and I. R. Hardy, Phys. Rev. B **45**, 7609 (1992).

[11] I. Etxebarria, R. M. Lynden-Bell, and J. M. Perez-Mato, Phys. Rev. B **46**, 13 687 (1992).

[12] V. I. Zinenko and D. H. Blat, Fiz. Tverd. Tela (Leningrad) **20**, 3539 (1978) [Sov. Phys. Solid State **20**, 2047 (1978)].

[13] H. M. James and T. A. Keenan, J. Chem. Phys. **31**, 12 (1959).

[14] V. G. Vaks, *Introduction in the Microscopic Theory of Ferroelectric Materials* (Nauka, Moskow, 1973).

[15] N. G. Zamkova and V. I. Zinenko, Fiz. Tverd. Tela (Leningrad) **34**, 2735 (1992) [Sov. Phys. Solid State **34**, 1464 (1992)].

[16] A. Huller and J. W. Kane, J. Chem. Phys. **61**, 3599 (1974); A. Huller, Z. Phys. **254**, 456 (1972).

[17] P. W. Fowler and P. A. Madden, Phys. Rev. B **29**, 1035 (1984).

[18] K. Binder, in *Monte Carlo Methods in Statistical Physics*, edited by K. Binder (Springer-Verlag, Berlin, 1979).

[19] D. P. Landau, Phys. Rev. **13**, 2997 (1976).

[20] W. M. Saslow, M. Gabay, and W. M. Zhang, Phys. Rev. Lett. **68**, 3627 (1992).

[21] K. Aiki, K. Hukuda, and O. Matumura, J. Phys. Soc. Jpn. **26**, 1064 (1969).

[22] M. Iizumi, J. D. Axe, G. Shirane, and K. Shimaoka, Phys. Rev. B **15**, 4392 (1977).

[23] N. Yamada and T. Ikeda, J. Phys. Soc. Jpn. **53**, 2555 (1984).